Available online at www.sciencedirect.com
ScienceDirect
ELSEVIER
Journal of Power Sources 163 (2007) 1091–1104
JOURNAL OF POWER SOURCES
www.elsevier.com/locate/jpowsour

Cycle life improvement of alkaline batteries via optimization of pulse current deposition of manganese dioxide under low bath temperatures

H. Adelkhani[a], M. Ghaemi[a,*], S.M. Jafari[b]

[a] Department of Chemistry, School of Sciences, Tarbiat Modarres University, P.O. Box 14115-175, Tehran, Iran
[b] Department of Mathematics, School of Sciences, Golestan University, Gorgan, Iran

Received 16 May 2006; received in revised form 17 September 2006; accepted 4 October 2006
Available online 7 November 2006

Abstract

Pulse current electrodeposition (PCD) method has been applied to the preparation of novel electrolytic manganese dioxide (EMD) in order to enhance the cycle life of rechargeable alkaline MnO_2–Zn batteries (RAM). The investigation was carried out under atmospheric pressure through a systematic variation of pulse current parameters using additive free sulfuric acid–$MnSO_4$ electrolyte solutions. On time (t_{on}) was varied from 0.1 to 98.5 ms, off time (t_{off}) from 0.25 to 19.5 ms, pulse frequencies (f) from 10 to 1000 Hz and duty cycles (θ) from 0.02 to 0.985. A constant pulse current density (I_p) of 0.8 A dm^{-2} and average current densities (I_a) in the range of 0.08–0.8 A dm^{-2} were applied in all experiments. Resultant materials were characterized by analyzing their chemical compositions, X-ray diffractions (XRD) and scanning electron microscopy (SEM). Electrochemical characterizations carried out by charge/discharge cycling of samples in laboratory designed RAM batteries and cyclic voltammetric experiments (CV). It has been proved that specific selection of duty cycle, in the order of 0.25, and a pulse frequency of 500 Hz, results in the production of pulse deposited samples (pcMDs) with more uniform distribution of particles and more compact structure than those obtained by direct current techniques (dcMDs). Results of the test batteries demonstrated that, in spite of reduction of bath temperature in the order of 40 °C, the cycle life of batteries made of pcMDs (bath temperature: 60 °C) was rather higher than those made of conventional dcMDs (boiling electrolyte solution). Under the same conditions of EMD synthesis temperature of 80 °C and battery testing, the maximum obtainable cycle life of optimized pcMD was nearly 230 cycles with approximately 30 mAh g^{-1} MnO_2, compared to that of dcMD, which did not exceed 20 cycles. In accordance to these results, CV has confirmed that the pulse duty cycle is the most influential parameter on the cycle life than the pulse frequency. Because of operating at lower bath temperatures, the presented synthetic mode could improve its competitiveness in economical aspects.

Keywords: Pulse electrodeposition; Duty cycle; Manganese dioxide; Rechargeable alkaline batteries; Cycle life; Bath temperature

1. Introduction

Research interest in the fundamental and functional properties of solid oxide electrodes provides informations, which can be used to improve the existing technology for further performance enhancement of electroactive materials. Of these, Manganese dioxide has attracted considerable attention owing to its use as the active material in environmental friendly RAM batteries [1–3]. One of the major demands for developing of this material is to modify and to strengthen the structural stability in order to prevent the rapid capacity fading during the process of charge/discharge cycling [4–7]. Additional demand is the reduction of bath temperature in commercial production of electrolytic manganese dioxide (EMD), which is carried out in boiling sulfuric acid solution. Since both the equipment and operational costs are high, advanced economical techniques must be developed with regard to its flexibility in control of process parameters.

Different types of electric currents and additives may enhance the physico-chemical properties of electroactive materials. These occur mainly through altering the concentrations of different species at the electrode surface, affecting charge and mass transfer kinetics [8–10]. Study of these processes may provide useful informations to explain their effects on electrochemical properties.

In our previous work, surface-active agents were introduced as additives into the electrodeposition bath to improve the desired electrochemical properties of EMD [11]. In practice, it is difficult and relatively expensive process to keep the amount

* Corresponding author. Tel.: +98 21 800 6631; fax: +98 21 800 9730.
E-mail address: ghaemi_m@modares.ac.ir (M. Ghaemi).

0378-7753/$ – see front matter © 2006 Elsevier B.V. All rights reserved.
doi:10.1016/j.jpowsour.2006.10.008

and quality of additives constant throughout the long time deposition process. Due to degradation of additives and incorporation of impurities, a prevailing non-uniform current distribution during nucleation process could not be prevented.

Pulse current deposition (PCD), as a new development in the area of battery technology, is reported to have the ability to tune the desired properties of materials instead of adding additives into the bath [12]. Therefore, it is important to optimize the appropriate pulse current (PC) conditions from among many available parameters. These conditions may be obtained by varying on time (t_{on}, period during which the potential is applied to the electrode), off time (t_{off}, the period during which no potential is applied) and peak current density (I_p), as independent variables [13].

Several studies of pulse deposition of electroactive materials are reported in the literature [14,15]. However, to the authors' knowledge, no systematic studies about correlations between the structural, morphological, and compositional properties of manganese dioxide with pulse parameters have been reported up to now.

PCD can be carried out with higher instantaneous current densities in comparison with direct current (DC) electrodeposition [16,17]. However, a previous study by the author has shown that most usual applied pulse parameters may be far from ideal in producing a better charge/discharge cycle performance of electrodeposits. Results actually showed that application of high I_p, can even decrease the performance of electrodeposited EMD [18]. In that work, we cited the influence of the pulse duty cycle (θ), where $\theta = t_{on}/(t_{on} + t_{off})$, as the main parameter affecting the electrochemical properties of deposits under conditions of a nearly constant average current density (I_a):

$$I_a = \frac{I_p t_{on}}{t_{on} + t_{off}} = I_p t_{on} f = I_p \theta \quad (1)$$

where pulse frequency (f) is the inverse of pulse period t_{pp} ($t_{pp} = t_{on} + t_{off}$).

It is necessary to pay attention to the fact that it is difficult to relate exactly the effect of pulse duty cycle to the properties of EMD if the peak current densities are changed. The most important parameter of PCD, which is directly related to changes in I_p is the anodic overpotential (η_a) [19,20]. High η_a, associated with high I_p, speeds up the nucleation leading to grain refinement. In this situation, the concentration of adatoms at the interface may be so high during a relative short t_{on} that there is not sufficient time for ordering them into a crystal lattice with the consequence that the regular crystal growth is inhibited. Application of higher I_p caused an increase of concentration polarization due to an increase of the reaction rate. Hence, an insufficient supply of the reacting species at the interface reduces the nucleation rate during the electrodeposition. Consequently, under low nucleation rate conditions, the grain size increased due to mass transfer limitations. In addition, high η_a has a strong influence on oxygen evolution reaction and microstructures of the anodically deposited oxide materials resulting in formation of crystal defects [21].

In an attempt to study the individual effects of pulse parameters on electrodeposit properties and to separate out the effects of high current densities, we tried to carry out all our experiments at different duty cycles and frequencies with keeping I_p constant and equal to DC current density. Under these conditions and application of sufficiently lower value of I_p we could be able to study the individual effects of pulse frequency on deposit properties [22]. Based on our previous study, the reason for choosing lower magnitude of I_p in the order of 0.8 A dm^{-2} is that at higher I_p, t_{on} and t_{off} both influence the electrocrystallization process effectively and consequently individual effects of t_{on} and t_{off} could not be studied [14,18]. In addition, application of constant I_p may offer the possibility of investigation of duty cycle effects more accurately because the extent of I_a variation at a constant I_p is much smaller than that of I_p at a constant I_a [12].

The aim of this work is a systematic study to better understanding of relative roles of pulse parameters directed at developing a new electroactive material to improve the cycle life of RAM batteries. Different series of EMD samples were produced by a careful choice of PC parameters. Characterization of pulse deposited MnO_2 are also described through relationships between pulse parameters and the perturbing of surface concentrations affecting the chemical composition of the EMD samples. For this study, the cation vacancy model of Ruetschi was used [23]. This model accounts for structural variety through the presence of lower valent Mn(III) ions and cation vacancies in the γ-MnO_2 structure:

$$(Mn^{4+})_{1-x-y}(Mn^{3+})_y(\square)_{2-4x-y}(OH^-)_{4x+y}$$

x represents the fraction of Mn(IV) ions, which are absent altogether. y and $\square$ represent the fractions of Mn(III) and cation vacancy, respectively. An appropriate number of protons located on adjacent oxide ions compensate the positive charge deficiency. Typical ranges for x and y are 0.06–0.08 and 0.04–0.12, respectively [24].

2. Experimental

2.1. Preparation of samples

Electrodeposition experiments were carried out in a 700 ml electrolytic cell kept at a constant temperature of 80 °C. A computer connected to a DC source was used to generate a rectangular pulse voltage signal of desired magnitude, duty cycle, and pulse frequencies. The bath composition is the regular additive free solution of manganese sulfate ($MnSO_4 \cdot H_2O$) 112 g l^{-1} and sulfuric acid (H_2SO_4) 100 g l^{-1}. All chemicals were purchased from Merck without further treatment. Deionized water was used for all experimental procedures. Electrolyte solution was stirred using a magnetic stirrer. A titanium plate (area: 1 dm^2) was used as the anode and Pb plates as the cathodes with a distance less than 7 mm between them. Details of the experimental set-up have been described elsewhere [18].

In the present work, the time interval between two-periodic pulses has been changed to vary θ between 0.02 and 0.98 as shown in Table 1. All experiments were performed at a constant peak current density (I_p) of 0.8 A dm^{-2} and the range of frequency studied is from 10 to 1000 Hz. Average current densities,

Table 1
The EMD electrodeposition conditions (pulse electrodeposition parameters, current densities and bath temperatures)

EMD samples	Frequency (f) (Hz)	Duty cycle (θ)	On-time, t_{on} (ms)	Off-time t_{off} (ms)	T_{on}/T_{off}	Pulse period, pp	Average current density ($A\ dm^{-2}$)	Bath temperature (°C)	n[a] in MnO_n	Label of corresponding batteries
Series 1										
M3	50	0.25	5	15	0.333	20	0.2	80	1.953	B3
M6	250	0.25	1	3	0.333	4	0.2	80	1.941	B6
M9	500	0.25	0.5	1.5	0.333	2	0.2	80	1.976	B9
M12	1000	0.25	0.25	0.75	0.333	1	0.2	80	1.944	B12
Series 2										
M2	50	0.025	0.5	19.5	0.03	20	0.02	80	1.946	B2
M5	250	0.125	0.5	3.5	0.143	4	0.1	80	1.918	B5
M9	500	0.25	0.5	1.5	0.333	2	0.2	80	1.976	B9
M13	1000	0.5	0.5	0.5	1	1	0.4	80	1.957	B13
Series 3										
M1	10	0.985	98.5	1.5	65.67	100	0.788	80	1.971	B1
M4	50	0.925	18.5	1.5	12.33	20	0.74	80	1.966	B4
M7	250	0.625	2.5	1.5	1.667	4	0.5	80	1.957	B7
M9	500	0.25	0.5	1.5	0.333	2	0.2	80	1.976	B9
Supplementary series										
M8	500	0.1	0.2	1.8	0.11	2	0.08	80	1.940	B8
$M9_{LT}$	500	0.25	0.5	1.5	0.33	2	0.2	60	1.910	$B9_{LT}$
$M9_{HT}$	500	0.25	0.5	1.5	0.33	2	0.2	98	1.950	$B9_{HT}$
$M10_{LT}$	500	0.5	0.1	1.90	0.05	2	0.4	60	1.918	$B10_{LT}$
M10	500	0.5	1	1	1.00	2	0.4	80	1.924	B10
M11	500	0.75	1.5	0.5	3.00	2	0.6	80	1.935	B11
M14	1000	0.75	0.75	0.25	3.00	1	0.6	80	1.972	B16
Mdc	DC	–	–	–	–	–	0.8	80	1.932	Bdc
Mdc_{HT}	DC	–	–	–	–	–	0.8	98	1.952	Bdc_{HT}

[a] Standard deviation = ±0.004.

in the range of 0.08–0.8 $A\ dm^{-2}$, could be changed by applied duty cycles. A charge of 2880 $C\ dm^{-2}$ was passed in each experiment. After deposition, all samples were mechanically removed from the Ti anode, rinsed with deionized water, ground with a pestle and mortar. The product was then sieved using 100 μm mesh screen and dried in an oven at 80 °C overnight. These samples were used for electrochemical tests, chemical analysis and X-ray diffraction analysis.

Three series of experiments were carried out with different pulse parameters but at a constant bath temperature of 80 °C (Table 1). The first set of experiments was aimed to observe the effects of pulse frequency on electrodeposits. Fixed values of 0.25 and of 0.33 were applied for duty cycle and t_{on}/t_{off} ratio, respectively. This value of θ was selected because of rather higher electrochemical activity of samples, produced in the initial stage of this investigation. The most uniform and smooth deposits (labeled as M9) obtained at a duty cycle of 0.25 and a pulse frequency of 500 Hz. Therefore, M9 was selected as the common sample belonging to all three series. This is due to better comparison of results in order to find a real trend in each series. In the next series, individual effects of variations of t_{off} and t_{on} was studied using the values of t_{on} and t_{off} applied for the synthesis of M9. The on duration for samples of series 2 was fixed at 0.5 ms and the variation of pause interval was set between 0.5 and 19.5 ms. The third series of experiment was carried out to investigate the effects of variation of t_{on} (between 0.5 and 99.5 ms) at a constant t_{off} of 1.5 ms.

Additional experiments with DC and PC currents were carried out at 80 °C as well as at higher and lower bath temperatures of 98 and 60 °C, respectively (Table 1, supplementary series). These experiments were done for the purposes of comparison and a better understanding of the effect of different pulse parameters as well as to study the economical aspects of this project.

2.2. Characterizations

Powder X-ray diffraction analysis was carried out by using a Philips X-ray diffractometer (model PW 1800) using Cu Kα radiation source operating at 30 kV. Each diffraction pattern was recorded in the 2θ range 10–80°, with a step size of 0.05 2θ and a count time of 2.5 s per step.

Current efficiencies (CEs) were measured by gravimetric weight differences before and after the electrodeposition using the following equation:

$$CE = \frac{n(W_{MnO_2}/M_{MnO_2})F}{I_a t \times 100} \quad (2)$$

where W is the weight of deposit (g), M the formula weight (85.4 $g\ mol^{-1}$), t the total deposition time (s), I_a average current density in PCD and current density in DC, n the valence of metal cation, and F is the Faraday constant.

Due to changes of bath compositions during a long time electrolysis and its possible effect on electrokinetics and surface morphologies, additional series of short time electrolysis experiments were carried on Ti foils under same conditions according to data given in Table 1. Total charge passed, in the order of 144 C dm^{-2}, was held constant in each experiment. The as-deposited samples were washed thoroughly with distilled water and dried in air for further study of surface morphology by Scanning Electron Microscopy (SEM, Philips model XL30).

Charge/discharge cycle performances of EMD samples were measured as the main cathodic component of laboratory designed RAM batteries. The constructions of these batteries were described elsewhere [18]. The weight of composite cathodes was 40 mg, prepared by mixing the EMD powder (90 wt.%), graphite (Lonza KS 44, 9.5%) and carbon black (0.5%). The mixture was pressed at 6 ton cm^{-2} for 10 min on stainless steel plates to form a cathode disc. Anode gels, which were similar in all test batteries, were extracted from rechargeable Pure Energy Batteries (Canada). Non-woven poly vinyl alcohol (PVA), consisting of two sheets of fibrous materials, served as matrix for the electrolyte and the PVA foil. Cycling experiments were performed using a home made computer-controlled battery-testing system. All cells have been discharged galvanostatically at a current density of 30 mAh g^{-1} MnO_2 and charged by voltage limited taper current (VLTC) method to 1.72 V. Discharge capacities were recorded to a cut-off voltage (COV) of 0.9 V. Each measurement was repeated at least two times with similar results and the reproducibility of the data was confirmed.

Cyclic voltammetry (CV) experiments were performed in 9 M KOH, with the aid of Potentiostat/Galvanostat (EG&G 273A) instrument using a three-electrode arrangement of a working electrode and platinum plate auxiliary electrode. The working electrode is composed of EMD/graphite powder mixture with a weight ratio of 2:98. This was mixed with sufficient 9 M KOH and pasted on a glassy carbon electrode (Ø: 2 mm). Voltamogramms are obtained after 5 cycles by sweeping the working electrode within a potential window of 0.85 to +0.4 V using a scan rate of 0.25 mV s^{-1} versus Hg/HgO reference electrode.

The value of n in MnO_n for each sample was determined using the potentiometric titration approach of Vetter and Jaeger [25]. 0.100 g of manganese dioxide sample was dissolved in 25.0 cm^3 of acidified 0.250 M $FeSO_4$ (10% H_2SO_4) to reduce all Mn(III) and Mn(IV) species to soluble Mn(II). MnO_n reduction with Fe(II) can be written as:

$$\mathrm{MnO}_n + (2n-2)\mathrm{Fe}^{2+} + (2n)\mathrm{H}^+ \rightarrow \mathrm{Mn}^{2+} + (2n-2)\mathrm{Fe}^{3+} + n\mathrm{H_2O}$$

Any Fe(II) remaining in solution after digestion can be potentiometrically back-titrated with 0.020 M $KMnO_4$ (V_1) to provide an indication of the amount of Mn(III) and Mn(IV) species present. Sufficient tetra sodium pyrophosphate ($Na_4P_2O_7\cdot 10H_2O$) was added to the titration vessel until the solution pH was in the range of 6–7. A second potentiometric titration was conducted using the same $KMnO_4$ solution, this time to determine the total manganese content of the sample V_2. The value of n in MnO_n was then calculated using:

$$n = 1 + \frac{5(V_0 - V_1)}{2(4V_2 - V_1)}$$

where V_0 is a replicate of the first titration in the absence of any sample. The standard deviation of n (in MnO_n) is in the order of 0.004.

The fraction of surface water (%H_2O_{su}) of each EMD sample was determined by heating 0.500 g (m_0) of the oxide in air in an oven at 110 °C for 2 h [24]. After cooling to ambient temperature in a desiccator, the weight was measured again (m_1). The sample was then heat-treated at 400 °C and re-weighed (m_2). The fractions of surface and structural water (%H_2O_{st}) contents can be calculated by:

$$\%\mathrm{H_2O_{su}} = 100\% \times \frac{m_0 - m_1}{m_0}$$

and

$$\%\mathrm{H_2O_{st}} = 100\% \times \frac{m_1 - m_2}{m_1}$$

The standard deviation for the measurement of surface and structural water was smaller than 0.039.

The cation vacancy fraction is also an indicator of the level of structural defects within γ-MnO_2. It can be calculated from the structural water (%H_2O_{St}) and total manganese content (%Mn_T) of the sample using:

$$x = 1 - \frac{2}{n+z}, \quad \text{where } n \text{ is the value in MnO}_n \text{ and}$$

$$z = \frac{54.94x(\%\mathrm{H_2O_{st}})}{18.016x(\%\mathrm{Mn_T})}$$

The total manganese content (%Mn_T) can be determined from the potentiometric titration used to determine V_2, i.e.:

$$\mathrm{MnO_4}^- + 8\mathrm{H}^+ + 4\mathrm{Mn}^{2+} + 15\mathrm{H_2P_2O_7} \rightarrow 5\mathrm{Mn(H_2P_2O_7)_3}^{3-} + 4\mathrm{H_2O}$$

Of course, takes into consideration the Mn^{2+} added as a result of the titration to determine V_1.

Mn(III) fraction (y) is determined using $y = 4 \times (2-n)/(2+m)$, where m is the ratio of moles H_2O per moles of Mn in EMD. Mn (IV) fraction was calculated via: Mn(IV) fraction = $1 - x - y$.

3. Possible relations between PCD parameters with deposition kinetics and the formation of crystal defects

The fundamental influence of pulse parameters on interactions between the manganese species, protons and water molecules on the electrode surface is important mainly through its ability to alter the kinetics of electrocrystallization process. Electrodeposition of manganese dioxide in acidic aqueous solution is believed to be affected essentially by the following successive steps [24,26,27]:

$$\mathrm{Mn_{sol}}^{2+} \rightarrow \mathrm{Mn_{ads}}^{3+} + \mathrm{e}^- \quad \text{(anodic oxidation)} \tag{3}$$

$$2Mn^{3+} + 2H_2O \leftrightarrow MnO_2 + Mn^{2+} + 4H^+$$

(disproportion reaction) (4)

The newly formed Mn^{2+} returns to the solution leaving a cation vacancy at the surface. The above oxidation process includes the formation of H^+ leading to a higher acidification of the anode surface compared to the acidity of the bulk solution.

Oxidation of Mn^{2+} on Ti electrode in the acidic solution (reaction (3)) may be initiated by hydroxyl radicals ($OH^\bullet$), which are produced through oxidation of water molecules at the anode surface [27]:

$$H_2O \rightarrow OH^\bullet + H^+ + e' \quad \text{(at Ti electrode)} \tag{3a}$$

OH radicals may react with Mn^{2+} ions to form Mn(III) species of the form $[Mn(OH_2)_5OH]^{2+}$, which is likely to exist as hydrated complexes $[Mn(OH_2)_6]^3$ in acidic medium [24]:

$$OH^\bullet + [Mn(OH_2)_6]^{2+} \rightarrow [Mn(OH_2)_5OH]^{2+} + H_2O \tag{3b}$$

$$[Mn(OH_2)_5OH]^{2+} + H^+ \leftrightarrow [Mn(OH_2)_6]^{3+} \tag{3c}$$

Reaction (3c) indicates that the stability of $[Mn(OH_2)_6]^{3+}$ increases with an increase in the acidity of the electrolyte solution. Generally, the fraction of Mn(III) ions in the γ-MnO_2 structure (y) can be interpreted as a competition between the rate of γ-MnO_2 deposition, the oxidizing power of the solution as well as the inherent stability of the Mn(III) species in the electrolyte media [24].

Charbe and Pannetier suggested a systematic way to characterize γ-Manganese dioxide by introducing "Pr", which represents the intergrowth of rutile-type pyrolusite (De Wolff disorder), within the ramsdellite structure. This defect controls to a large extent the mechanism of reduction and proton intercalation. Microtwinning (Tw), which represents the number of faults generated by twinning [3], was shown to be associated with the Mn^{4+} vacancies generated by oxygen evolution during MnO_2 electrodeposition [28].

Electro-oxidation of manganese adsorbed on the electrode surface can be explained qualitatively in terms of the rate of Mn^{3+} formation and the rate of disproportionation reaction with the assumption that the latter is the rate-determining step in the overall mechanism. If the rate of reaction (3) becomes much higher, the reaction (4) is not any more capable to consume all the Mn^{3+} formed giving rise to accumulation of Mn^{3+} species on the electrode surface. In this case, the probability for incorporation of these species and formation of a twin becomes energetically more favorable. However, one should bear in mind that a certain amount of microtwinning and cation vacancies would be beneficial to the migration of protons that may result in an increase of the conductivity and thus electrochemical activity. In addition, high deposition rate of γ-MnO_2 may lead to an increasing trend of H_2O inclusion into the lattice. EMD generally contains ~4 wt.% of structural water in the lattice, which dramatically influences not only electrochemical properties but also other properties such as the density and the electronic conductivity [29].

Pulse parameters may affect the kinetics that one or other parameter may become more important to modify the structural and/or compositional features of deposits. This is because of combined effects of pulse parameter t_{on}, t_{off}, pulse frequency and duty cycle on deposit properties, which could be additionally affected by physico-chemical characteristics of electrode substrate and electrolyte solution. Hence, the measured individual effects of each pulse parameter must be regarded as an approximate data in order to find the optimum condition. In general, this condition is given when $t_{off} \geq$ discharging time of the electrical double layer [21]. The off duration should also be as long as necessary to allow ion transport into the depleted vicinity of the electrode surface. On time must be sufficiently long to fully charge the electrical double layer (t_c) [30].

4. X-ray diffraction

Fig. 1 shows the XRD patterns of a group of pcMDs fabricated through modulating of duty cycle from 0.1 to 0.75 while fixing the frequency at 500 Hz. Two distinct reflections (0 0 2) and (0 6 1) in the range $64° < 2\theta < 71°$ as well as relative higher sharpness of the line (1 3 0) (at $2\theta \approx 56°$) indicate a less microtwinned

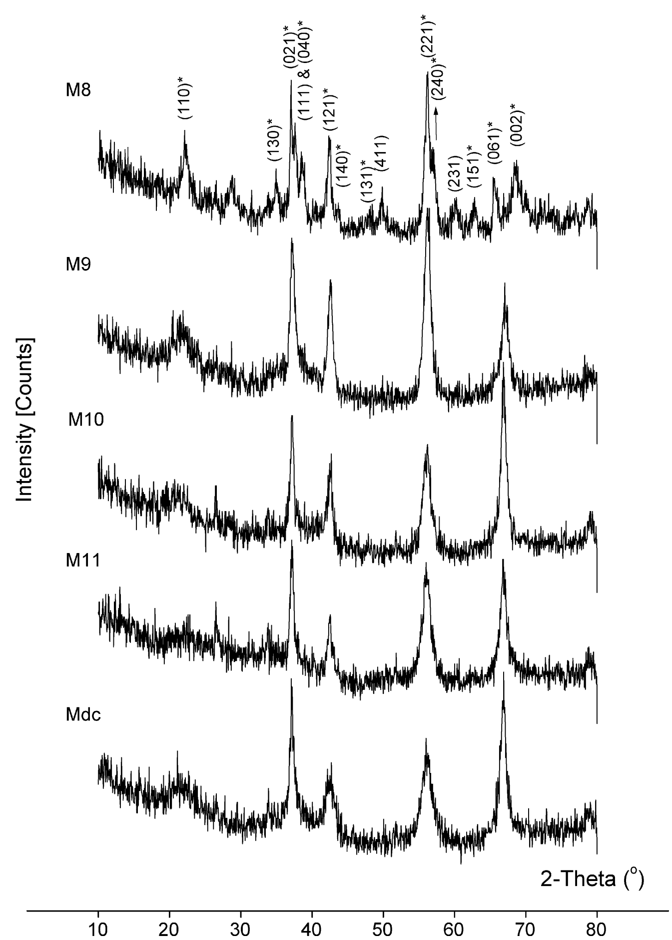

Fig. 1. X-ray diffraction pattern of EMD sample deposited by direct current (Mdc) and a group of pcMDs electrodeposited at a fixed pulse frequency of 500 Hz and different duty cycles: $\theta = 0.1$ (M8); $\theta = 0.25$ (M9); $\theta = 0.5$ (M10) and $\theta = 0.75$ (M11). Peaks marked with an asterisk correspond to ramsdellite phases.

structure of M8 compared to other samples [31]. In general, microtwinning induces a merging of both (2 2 1) and (2 4 0) lines (at $2\theta \approx 56^\circ$) and of the (0 0 2) and (0 6 1) lines at (at $2\theta \approx 65^\circ$) into combined peaks. According to Ref. [31], M8 may not belong to type I samples, for which the present amount of Tw is less than 50%. The explanation is that the doublet (2 2 1/2 4 0) is not clearly separated and mix crystals of α-/β-MnO_2 are also present within the γ-MnO_2 structure of M8. Pyrolusite impurities could be seen through the presence of a weak reflection at 28.7° in 2θ as well as by a slightly shift of the (1 1 0) line to higher angle (at $2\theta = 22.1^\circ$) compared to that of a defectless ramsdellite (at $2\theta = 21.8^\circ$) (De Wolff disorder) [31,32]. The presence of α-MnO_2 (indicated at least by two reflections given by Miller indices "*h k l*", which are not marked with asterisk), may be attributed to the incorporation of metal ion impurities such as K^+ and Ba^{2+} during a relatively long t_{off}. These phenomena, affect the surface diffusion of adatoms, which may influence their incorporation to new crystallites and formation of thermally stable α-MnO_2. All samples, with exception of M8, exhibit only two broad and symmetrical lines in the range 54–71° and could be categorized as type III samples [31].

Fig. 1 shows that the XRD pattern of the sample M11 is very similar to that of the Mdc, the only significant difference being the more diffuse and broad peak at ∼22° 2θ indicating a rather amorphous and defective material. It could be observed that the sharpness of line (1 1 0) decreases with increasing duty cycle (from M8 to M11). In this regard, one may assume that the value of I_a may be responsible for the appearance of such a phenomenon, as I_a has been increased with increasing duty cycle from M8 ($0.08\ A\ dm^{-2}$) to M11 ($0.6\ A\ dm^{-2}$). This assumption is based on the results of preisler reporting that the "sharpness" of line (1 1 0) decreases rapidly with increasing deposition current density (DCD) [31]. However, in spite of higher applied DCD in Mdc ($0.8\ A\ dm^{-2}$), the sharpness of line (1 1 0) is higher than that of M11 ($I_a = 0.6\ A\ dm^{-2}$). This indicates that other parameters of pulsating current are responsible for the appearance of such effect. Results of our previous work has shown that the electrochemical behavior is mainly affected by I_p and pulse duty cycle [18]. Obviously, optimized applied θ in M9 prevents the formation of mix crystals. Nevertheless, higher amount of Tw is also present in M9. This is indicated via disappearance of line 130, which has become broad and shifted to larger diffraction angles in such a way that it is now almost hidden below the line (0 2 1) [31]. At this stage of investigation, the relative amount of Tw in M9 is not exactly clear, as the sharpness of line (1 2 1) at $2\theta \approx 42^\circ$, which is not affect by De Wolff disorder [33,34] and the intensity of line (1 1 0) is higher than other pcMDs (Fig. 1). Anyhow, the higher intensity of the latter peaks and the preferentially growth along [2 2 1]/[2 4 0] direction at $2\theta \approx 56^\circ$ are indications for the higher crystallinity of M9 compared to Mdc and to other pcMDs produced at $\theta > 0.25$.

5. Influence of pulse parameters (f, t_{off}, t_{on}) and the role of pulse duty cycle on physico-chemical properties of deposits

5.1. Effects of pulse frequency

Fig. 2 shows the morphologies of pcMDs of series 1 obtained at frequencies of 50, 250, 500 and 1000 Hz at a constant average

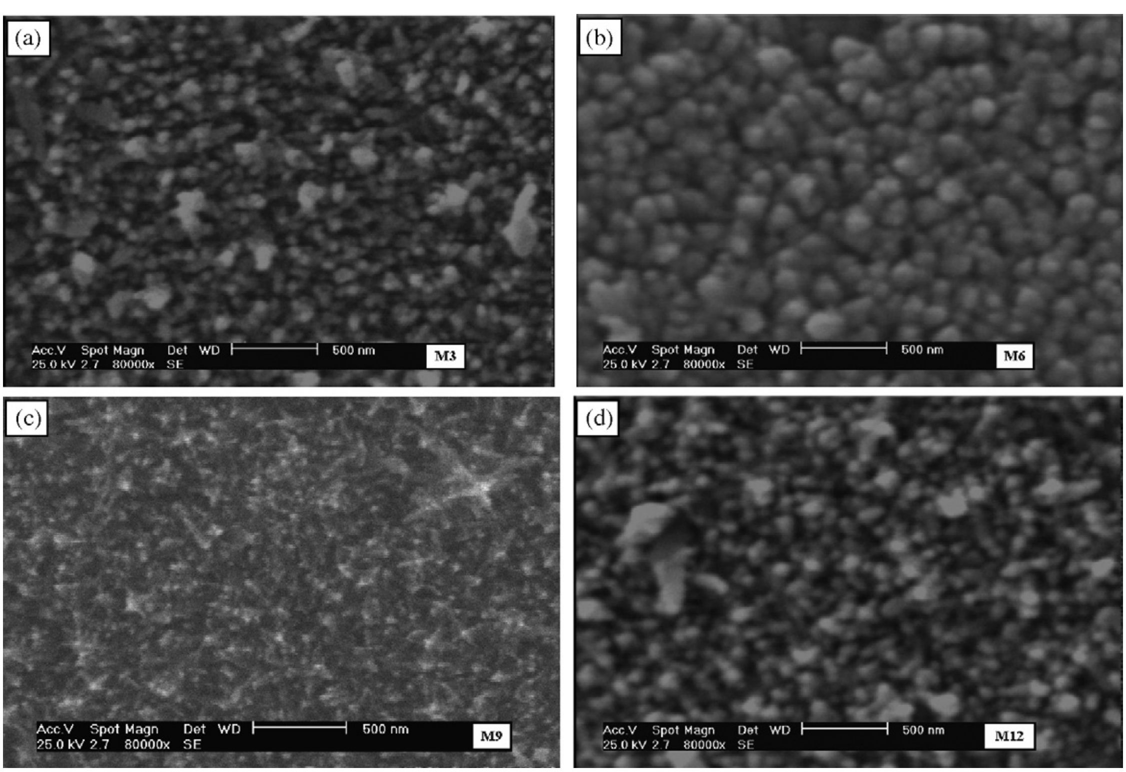

Fig. 2. SEM images show the effects of different pulse frequencies on microstructures of pcMDs of series 1 synthesized at a fixed duty cycle of 0.25. (a) $f = 50$ Hz; (b) $f = 250$ Hz; (c) $f = 500$ Hz, and (d) $f = 1000$ Hz.

current density of 0.2 A dm^{-2} and a fixed duty cycle of 0.25. As the peak current density, average current density and duty cycle are equal for all deposits, the change in physicochemical properties is related to the values of the frequencies. Among all pcMDs in this series, M6 (Fig. 2b) presented relative larger spherical particles of approximately 85 nm. By increasing the frequency from 250 to 500 Hz, more fine deposit is observed as in the case of M9. The latter, has a seemingly higher compactness and uniformity. Further increase of frequency to 1000 Hz (M12) causes the morphology to become similar to that of M3. Obviously, the effects of longer t_{on} and t_{off} at low pulse frequency (M3), on the nucleation and growth mechanism, is similar to that of shorter t_{on} and t_{off} at high pulse frequency (M12).

Fig. 3a shows that the fraction of cation vacancy and Mn^{4+} increases to its highest level at a frequency of 500 Hz (M9). Clearly, any Mn^{3+} within the structure is available through the removal of a Mn^{4+} ions and insertion of a proton. Hence, an opposite trend was observed for the amount of Mn^{3+}.

Concerning water fractions of samples, Fig. 4a shows that M9 exhibits a relatively lower amount of H_2O_{surf} and higher one for H_2O_{struct} among samples of series 1. As could be seen in Fig. 4, the extent of these variations induced by pulse frequency is lower than the effect of duty cycles on different type of water fractions.

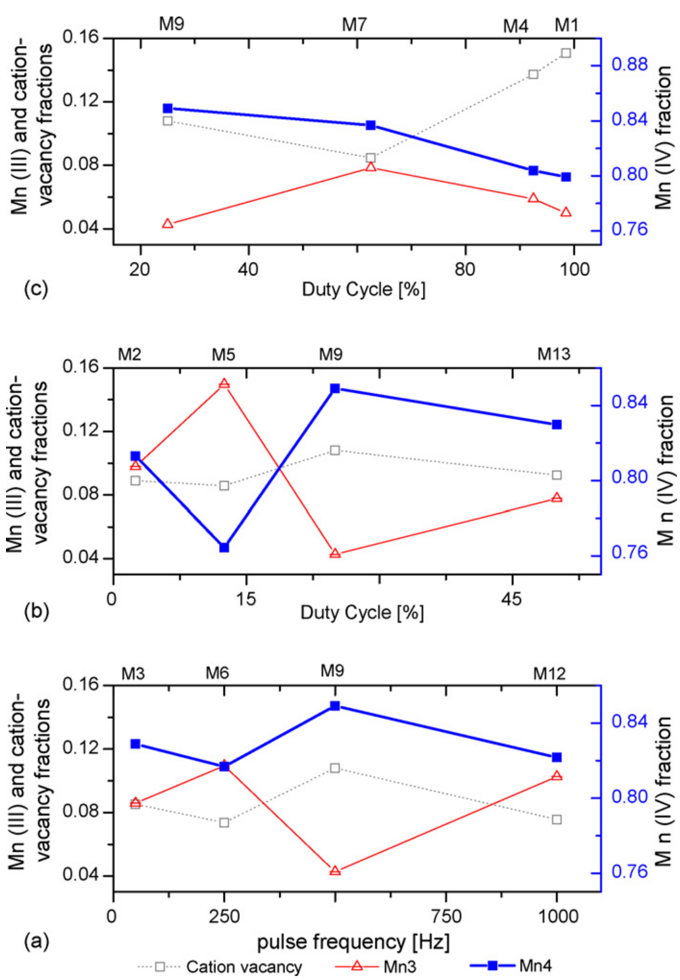

Fig. 3. (a) Effects of pulse frequency on chemical compositions of pcMDs (series 1). (b) Effects of pulse duty cycles on chemical compositions of pcMDs (series 2) and (c) series 3.

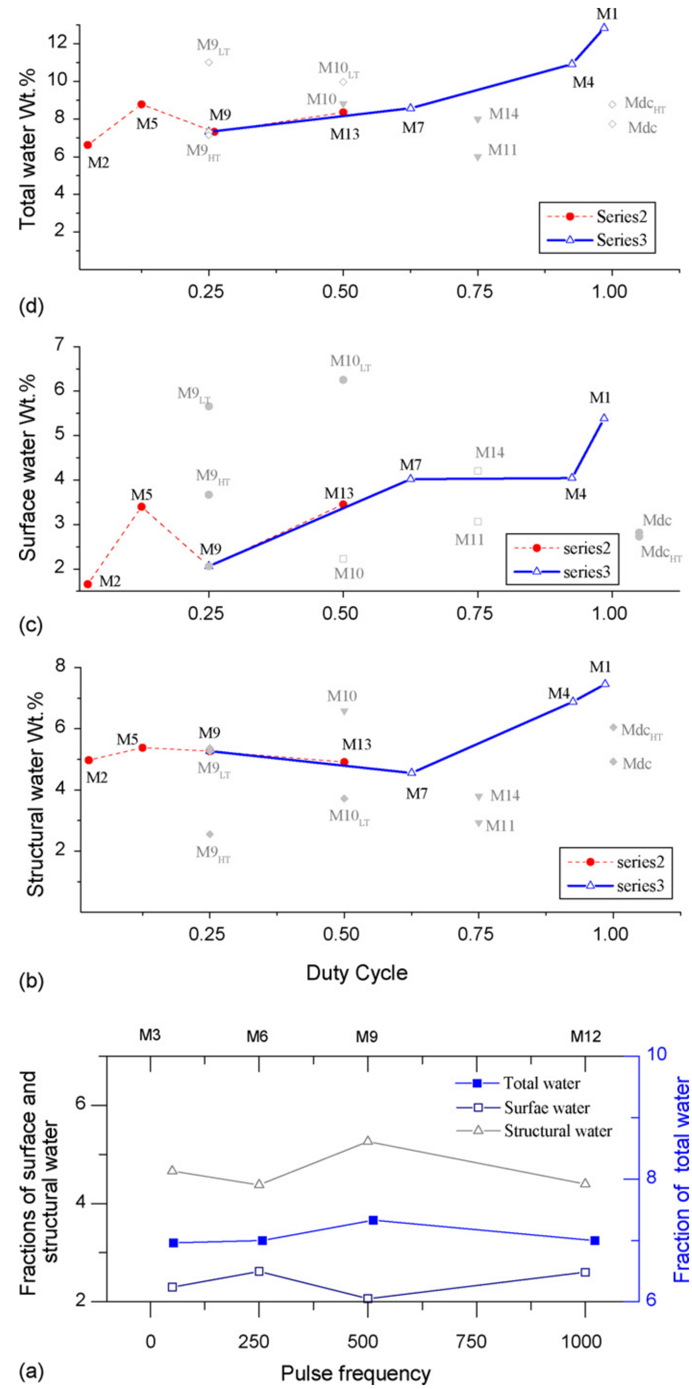

Fig. 4. (a) Effects of pulse frequencies on water content of pcMDs of series 1. (b) Effects of pulse duty cycles on structural water, (c) surface water and (d) total water content of series 2 and 3 (standard deviation = ±0.039).

5.2. Effects of off time

The effects of t_{off} on the chemical compositions and water contents of different pcMDs are given in Figs. 3b and 4, respectively. It may be assumed that during the long off period (as in the case of M2), existing grains become unstable. This favors smaller clusters of Mn(III) and Mn(IV) species (with their hydrated water molecules), which are of lower thermodynamically stability, to be dissolved into the bath. Consequently, not only a general decrease of current efficiencies (Section 5.5) but also a decrease of incorporated water molecules could be expected. With decreasing t_{off} (as in the case of M5), the electrochemically fresh nucleated species have not sufficient time to be dissolved into the solution. It is supposed that in the case of M5 the acidity of the electrode surface is sufficient to stabilize the Mn(III) species but not enough for a further total oxidation to Mn(IV). The lower value of n measured for M5 (Table 1) confirmed this supposition. This condition would lead to accumulation of Mn^{3+} species on the electrode surface and their facilitated incorporation into the EMD lattice (Fig. 3b).

At optimized duty cycle and lower off time applied in the synthesis of M9, the relative acidity on the electrode surface is higher. Therefore, the power for oxidizing of Mn^{3+} is increased and the probability of incorporation of Mn^{3+} ions into the lattice is decreased. Under these conditions, the rate of soluble Mn(III) formation and its stability is such that the conversion to β-MnO_2 (formation of De Wolff disorder) is optimized [24]. As could be observed in Fig. 3a–c, M9 has the minimum amount of Mn^{3+} and middle fraction of cation vacancies among all samples produced at a bath temperature of 80 °C.

5.3. Effects of on time

The effect of the variation of t_{on}, from 0.5 to 98.5 ms at a constant off time of 1.5 ms on the compositions and water contents of pcMDs (series 3) is depicted in Figs. 3c and 4, respectively. The measured amount of Mn^{4+} has a decreasing trend with increasing duty cycles. M1 and M4, which are produced at $\theta > 0.9$, have a high content of water and nearly the same chemical compositions. Obviously, longer t_{on} than a few three milliseconds causes a decrease in the fraction of Mn^{4+} possibly due to insertion of water molecules. This would facilitate

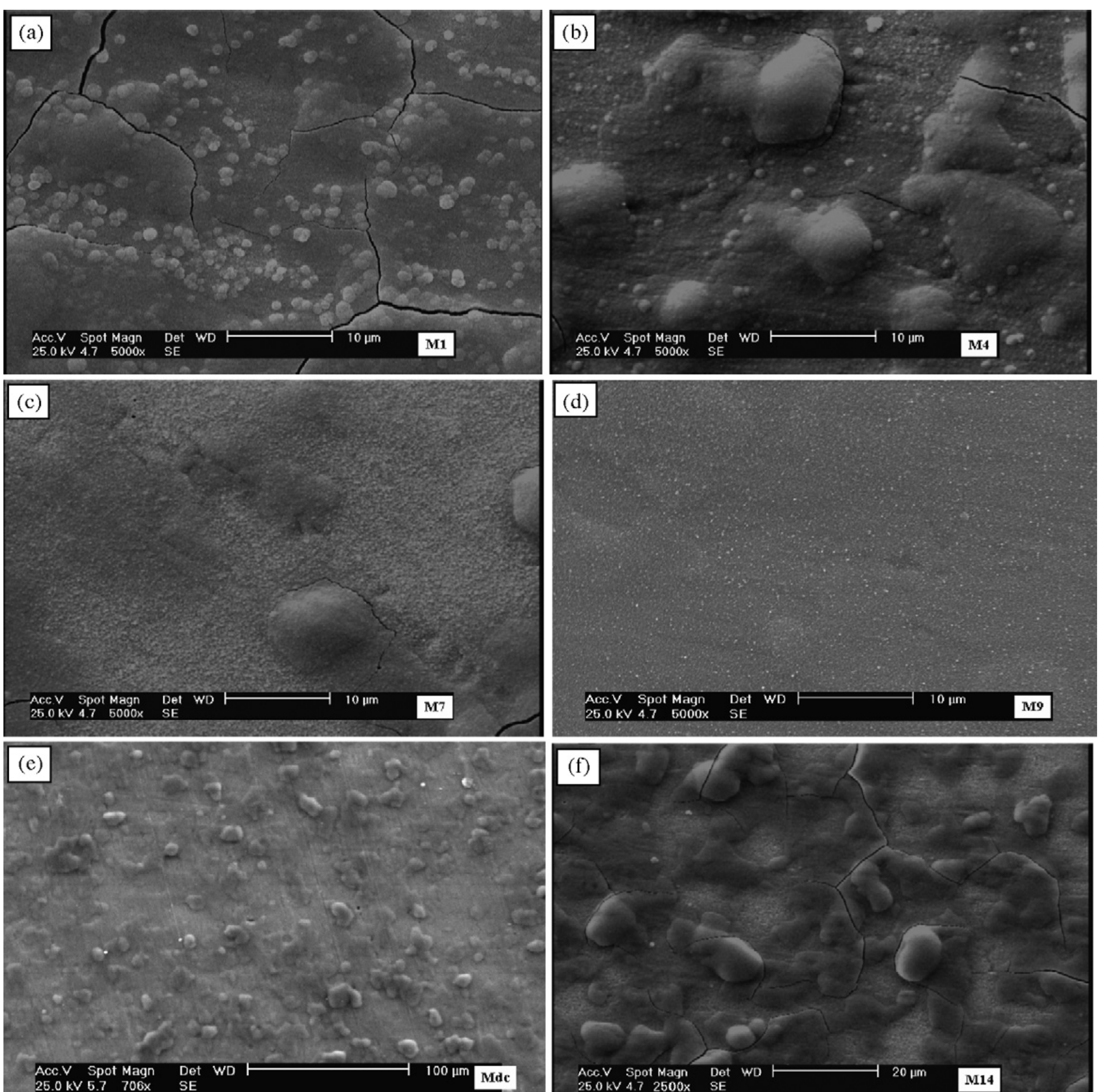

Fig. 5. SEM images of pcMDs of series 3 (a–d) electrodeposited at a constant off time of 1.5 ms and different on times (a) $t_{on} = 98.5$ ms, $f = 10$ Hz; (b) $t_{on} = 18.5$ ms, $f = 50$ Hz; (c) $t_{on} = 2.5$ ms, $f = 250$ Hz; (d) $t_{on} = 1.5$ ms, $f = 500$ Hz; (e) SEM image of Mdc; (f) SEM image of M14 ($\theta = 0.75$, $f = 1000$ Hz, $t_{on} = 0.75$ ms and $t_{off} = 0.25$).

an easier transport of protons replacing Mn^{4+} ions and creating more cation vacancies (M1 and M4 in Fig. 3c). Higher amount of incorporated water may decrease the structural strength leading to a possible crystal collapse induced by volume pulsation during charge/discharge cycling. In addition, incorporation of excessive amount of H_2O at sufficient surface acidity may decrease the O_2 evolution overvoltage. Under these conditions, the probability for the formation of Tw defects in EMD crystal lattice is higher. Hence, we may expect a relative lower electrochemical cycle performance especially in the case of M1 and M4 of series 3 (Section 6.1, Fig. 11).

It is supposed that the depletion of Mn^{2+} ion concentration in the vicinity of the electrode surface could not be recovered sufficiently during the shorter t_{off} (high duty cycle). Therefore, the process becomes to some extent diffusion-controlled under lower nucleation rate. This condition may lead to formation of relatively large spherical and three-dimensional grains (Fig. 5a). As shown in Fig. 5, M1 and M4 presented cracks whereas M9 (θ: 0.25, Fig. 5d) showed a stress free and smooth surface. This suggests that the optimized t_{on} (in accordance to an optimum value of t_{off} and hence pulse duty cycle) may reduce the mass transfer problem resulting in a decreased formation of internal stress.

Anyway, the importance of pulse duty cycle on surface morphologies could be realized if we consider the morphology of M14 (Fig. 5f, f: 1000 Hz, θ: 0.75). Synthesis conditions under high pulse duty cycle (specially at high applied frequencies) causes that the morphology becomes similar to that of Mdc (Fig. 5e). The dull appearance and uneven surface with a tendency for stress formation are typical characteristics of pcMDs with similar physicochemical and electrochemical properties as those obtained by DC electrodeposition.

5.4. Effects of bath temperatures

Fig. 6a shows that for dcMDs there is a trend towards a lower y (Mn^{3+}) value at higher bath temperatures. This indicates that the disproportionation step in the mechanism, leading to MnO_2 is efficient [24]. However, in PCD the situation is different for different ranges of temperatures if we consider the lower Mn^{3+} (y) fraction of M9 compared to $M9_{LT}$ (Fig. 6b). The higher level of cation vacancies of the latter is related to the higher amount of physical water and easier transport of protons, replacing Mn^{4+} ions. With increasing bath temperature from 80 to 98 °C, a slightly increasing trend of Mn(IV) as well as oxygen content are observed for both dcMDs and pcMDs (Table 1).

Different trends of changes of the H_2O_{surf} and H_2O_{struct} fractions are observed for pcMDs and dcMDs with increasing bath temperatures. Fig. 4c shows that increasing bath temperature from 80 to 100 °C has in fact no significant effects on the amount of H_2O_{surf} among dcMDs, whereas the fraction of H_2O_{surf} of $M9_{HT}$ has been increased compared to M9. For dcMDs, we measured an increasing trend of H_2O_{struct} with increasing bath temperatures from 80 to 98 °C, whereas a reversed trend is observed for pcMDs (M9 and $M9_{HT}$ in Fig. 4b). In addition, the increasing trend of H_2O_{struct} from M10 to $M10_{LT}$ (at θ: 0.5)

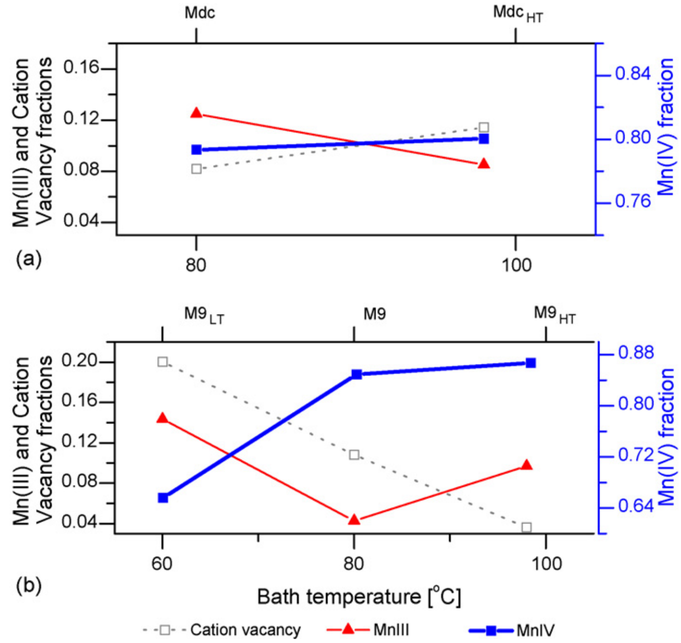

Fig. 6. (a) Effects of bath temperatures on chemical composition of DC electrodeposited samples at a bath temperature of 80 °C (Mdc) and in boiling bath solution of 98 °C (Mdc_{HT}). (b) Effects of bath temperatures on chemical compositions of pcMDs electrodeposited at fixed values of f = 500 Hz, θ = 0.25 at different bath temperatures of 60 °C ($M9_{LT}$), 80 °C (M9) and in boiling bath solution of 98 °C ($M9_{HT}$).

is not observed for M9 to $M9_{LT}$. This indicates that the influence of bath temperature is connected with the effect of pulse duty cycle on the water content and other physico-chemical properties of pcMDs.

5.5. Effects on current efficiencies (CE)

Fig. 7 shows the maximum efficiency obtained for Mdc was in the order of 96% and the minimum was 35% for M2. With a

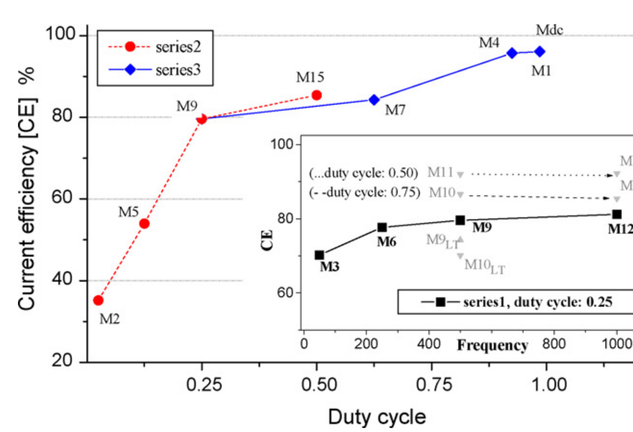

Fig. 7. Influence of pulse duty cycles on current efficiencies of pcMDs of series 2 (fixed t_{on} of 0.5 ms and different t_{off}) and series 3 (fixed t_{off} of 1.5 ms and different t_{on}). Inside graph shows the influence of pulse frequencies on pcMDs current efficiencies of series 1 (fixed duty cycle of 0.25) and two pairs of pcMDs produced at fixed duty cycles of 0.5 (M11, M14) and a duty cycle of 0.75 (M10, M13). Inside graph shows also the influence of bath temperatures for pcMDs produced at fixed duty cycles of 0.25 ($M9_{LT}$ M9, $M9_{HT}$) and a fixed duty cycle of 0.5 ($M10_{LT}$ and M10).

given duty cycle of 0.25 (series 1), CE increased approximately 10% as the frequency increased from 50 to 1000 Hz attaining a value of 81% at 1000 Hz (inside graph of Fig. 7). The fact that at high pulse frequencies the double layer does not fully charge during the t_{on} or fully discharge during the t_{off} leads to a condition where the current fluctuates around the average current density [35]. This means the deposition behaves more like ripple DC, with like wise higher values of CEs. We may assume that under DC conditions or under PCD with higher θ values, high concentrations of sulfuric acid are available on the electrode surface, which is a beneficial factor for dissolved oxygen to oxidize the lower valence manganese species, resulting in apparently larger current efficiencies.

However, if we consider three pairs of pcMDs M9, M12; M10, M13 and M11, M14 (inside graph of Fig. 6), we see that increasing pulse frequency from 500 to 1000 Hz at fixed duty cycles, have a negligible effect on current efficiencies. In addition, we have measured actually an opposite trend in CE with increasing frequency of series 3 compared to series 1. These results indicate that the effect of duty cycle on CEs is more efficient than the effect of pulse frequency.

We can notice that lower t_{on}/t_{off} ratios (low pulse duty cycles as in the case of M2, series 2) have decisive roles in lowering the current efficiencies. Long off period between the current pulses allows decay of overpotential below the activation values. Thus, during t_{off}, with the cessation of the growth process, regions of crystallites protruding away from the deposited surface as well as adsorbed nuclei are more prone to undergo desorption process [36]. In this connection, Cheh et al. have argued that for complex reaction systems involving two consecutive reaction steps, PCD favors the first step in the reaction sequence, resulting in a loss of current efficiencies [37,38].

6. Electrochemical tests

6.1. Laboratory test batteries

Fig. 8 shows the effects of pulse frequency on discharge capacities of electrodes fabricated by pulse electrodeposition for a given duty cycle of 0.25. It could be shown that the capacities of all pcMDs are comparable in the first 5 cycles. However, deviations of capacities are measured particularly for B12 as the cycling proceeds. The latter shows a lower potential drop and higher capacities up to 30th cycle. This result would be desirable for a battery material because present trends in battery requirements are toward higher power. M9 has displayed a longer cycle life, but it has a comparatively slightly lower capacities during the early cycles compared to M12. This trend likely reflects the competing effects of modified structural stability through the probable presence of α- and/or rutile type pyrolusite and the electrochemical activity of γ-MnO_2. The effect of increasing pulse frequency from 500 to 1000 Hz for two pair of samples, which are produced at fixed duty cycles of θ: 0.25 (M10, M13) and θ: 0.75 (M11, M14) on discharge capacities are shown in Fig. 9. Whereas B10 has higher capacities up to 20th cycle, B13 shows lower capacities but the rate of decrease in capacities is lower and the cycle life is higher compared with B10. Under

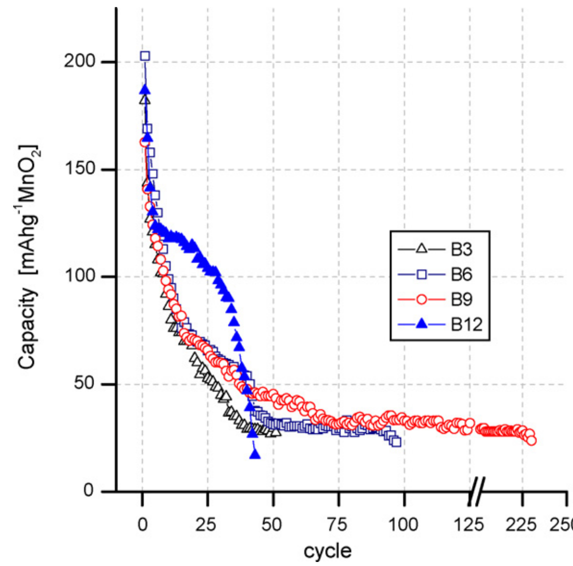

Fig. 8. Discharge capacities of laboratory designed RAM batteries based on EMD electrodeposited at a fixed duty cycle of 0.25 and different frequencies: 50 Hz (B3); 250 Hz (B6); 500 Hz (B9) and 1000 Hz (B12).

application of higher duty cycles in the order of $\theta \geq 0.75$, the effect of pulse frequency on cycle performances is very low, as the performance of both samples (B11 and B14) are strongly reduced. Lower cycle life of B11 may be caused by the lower degree of crystallinity and the presence of higher amount of crystal defects, as indicated by XRD pattern (Fig. 1). The cycle life of the latter is comparable to that of Mdc.

In series 2, we observe that the energy drawn from B13 during the first 40 cycles is higher than other samples (Fig. 10). In comparison, samples prepared at low duty cycles such as M2 (θ: 0.025) and M5 (θ: 0.125) exhibit inferior electrochemical performances. This may be attributed to the presence of crystal defects and the existence of mix crystals. As we saw in Fig. 1,

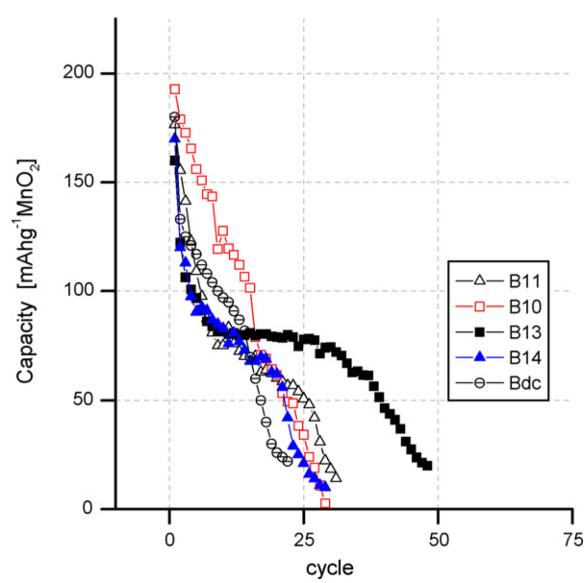

Fig. 9. Influence of pulse frequency on discharge capacities of two pair of RAM batteries based on EMDs electrodeposited at different frequencies of 500 and 1000 Hz but fixed duty cycles of 0.5 (M10 and M13) and 0.75 (M11 and M14).

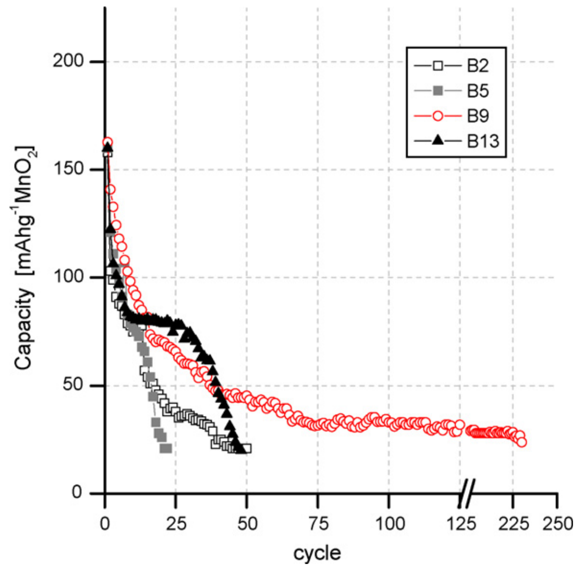

Fig. 10. Discharge capacities of batteries based on EMD electrodeposited at a fixed on time (t_{on} = 0.5 ms) and different off times (series 2).

XRD has confirmed this phenomenon for M8 (θ: 0.1, f: 500 Hz) as an example for samples produced under lower values of pulse duty cycles.

No significant deviation in discharge capacities can be observed in B9 and B7 (cycle life: 110) during the early 25 cycles (Fig. 11, series 3). Thereafter, B7 exhibits a higher rate of increasing capacities up to 90th cycle. After 90th cycle, the rate of capacity fading is higher for B7 compared to B9. The lower performances of B1 and B4 are attributed to their higher content of cation vacancies and water causing structural instability during charge/discharge cycling.

In order to study the effect of bath temperature, additional experiments for the synthesis of M9 were carried out at higher and lower bath temperatures of 98 °C ($M9_{HT}$) and 60 °C ($M9_{LT}$),

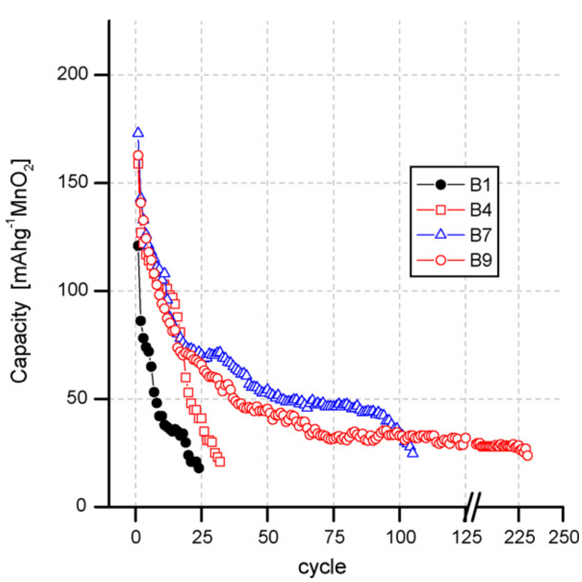

Fig. 11. Discharge capacities of RAM batteries based on EMD electrodeposited under constant off time of 1.5 ms and different on times (series 3).

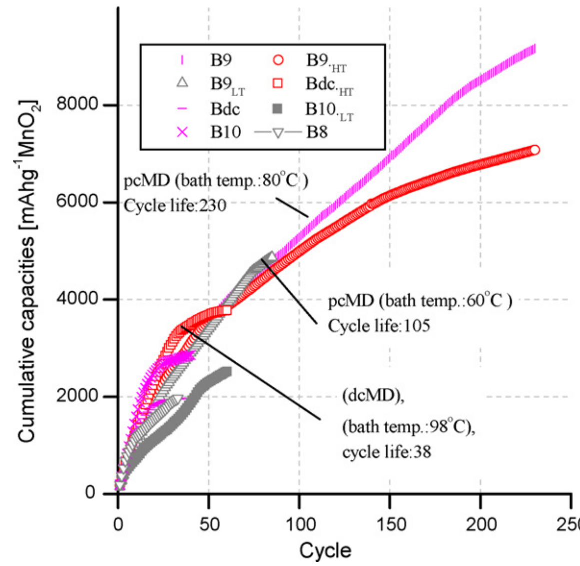

Fig. 12. Cumulative capacities of RAM batteries based on EMD electrodeposited under different pulse and DC conditions (see Table 1, supplementary series).

respectively. Fig. 12 shows that application of higher bath temperature than 80 °C did not bring any improvements in electrochemical cycle performances under our experimental conditions. The cycle life of $B9_{HT}$ (100 cycles) was even lower than B9 (230 cycles). For the purpose of comparison with B9, all measured cycle capacities of $B9_{HT}$, including those lower than 30 mAh g^{-1} MnO_2 (cycles 100–230) are included in Fig. 12. DC deposition at 60 °C was not successful at Ti anode under the same conditions as for Mdc. This could be attributed to higher surface concentration of hydroxyl radicals, which may preferably react at lower bath temperature with each other to produce O_2. The gas evolution impairs the adhesion of deposits to Ti substrate. Another explanation for this phenomenon is the formation of passive layer of TiO_2 at lower temperatures. Under these conditions, the activation energy is presumably too large to allow a rapid structural conversion to β-MnO_2 and adhesion to substrate. We suggest that the synthesis of $M9_{LT}$ was possible due to higher overvoltage for oxygen evolution and a possible formation of β-MnO_2 on TiO_2 substrate, which has the same rutile type structure. Further investigation is necessary to clarify these phenomena.

As shown in Fig. 12, Bdc_{HT} shows slightly higher initial cumulative discharge capacities compared to $B9_{LT}$. After nearly 40 cycles, the cumulative capacities of Bdc_{HT} are strongly reduced. This result show the possibility of both improving the cycle life of RAM batteries and a reduction of bath temperature at least in the order of 40 °C, using optimized PCD conditions. Samples produced at lower duty cycles like M8 (θ: 0.1) exhibit slightly higher initial capacities in early cycles, which may be related to lower amount of twinning defects. The drop in capacity of such sample after a few cycles is maybe a consequence of the presence of mix crystals, which could contribute to structural collapse during charge/discharge cycling.

We suppose that the cycle life enhancement is correlated to higher structural stabilities of EMDs. It is assumed that the presence of fine distributed micro/nanoparticles of α-MnO_2 and/or β-MnO_2 within a γ-MnO_2 structure may be a major factor in evaluation of the γ-MnO_2 stability for achieving a higher number of cycle life. This assumption is supported from the fact that firstly, during t_{off} adsorption of impurities (originated from the electrolyte) could take place. These impurities like K^+, Na^+ may contribute to the formation and stabilization of α-MnO_2. Secondly, if the current is interrupted during electrodeposition, then γ-MnO_2 may undergo a transition to β-MnO_2 [24].

We may conclude from the results of test batteries of three couple of pcMDs produced at 500 and 1000 Hz (B9, B12; B10, B13 and B11, B14) that the ratio of the pulse off time to the pulse on-time, manifested by duty cycle, is more influential on the electrochemical performances than pulse frequency. As a consequence, for experiments which could be carried out at different current densities, after fixing of an optimum duty cycle, the frequency can be modulated to tune the desirable characteristics of deposits regarding its electrochemical energy, rate of capacity fading and cycle life.

6.2. Cyclic voltammetry

CV experiments were carried out for Mdc and two groups of pcMDs, which are produced at fixed pulse frequencies of 500 Hz (Fig. 13) and 1000 Hz (Fig. 14), respectively. The reduction process of EMD occurs in three main steps identified in the range of 0–0.4 V [31]. These are believed to correspond to the homogeneous solid-state reduction of proton insertion into the channels of ramsdellite and pyrolusite domains of γ-MnO_2. Continuing the potential sweep to more negative values than −0.4 V causes the formation of a solution-based Mn(III) intermediate via dissolution of MnOOH to subsequently precipitation of pyrochroite $Mn(OH)_2$ [39]. For γ-MnO_2 samples, the higher capacity of this process is usually associated with higher surface area and hence

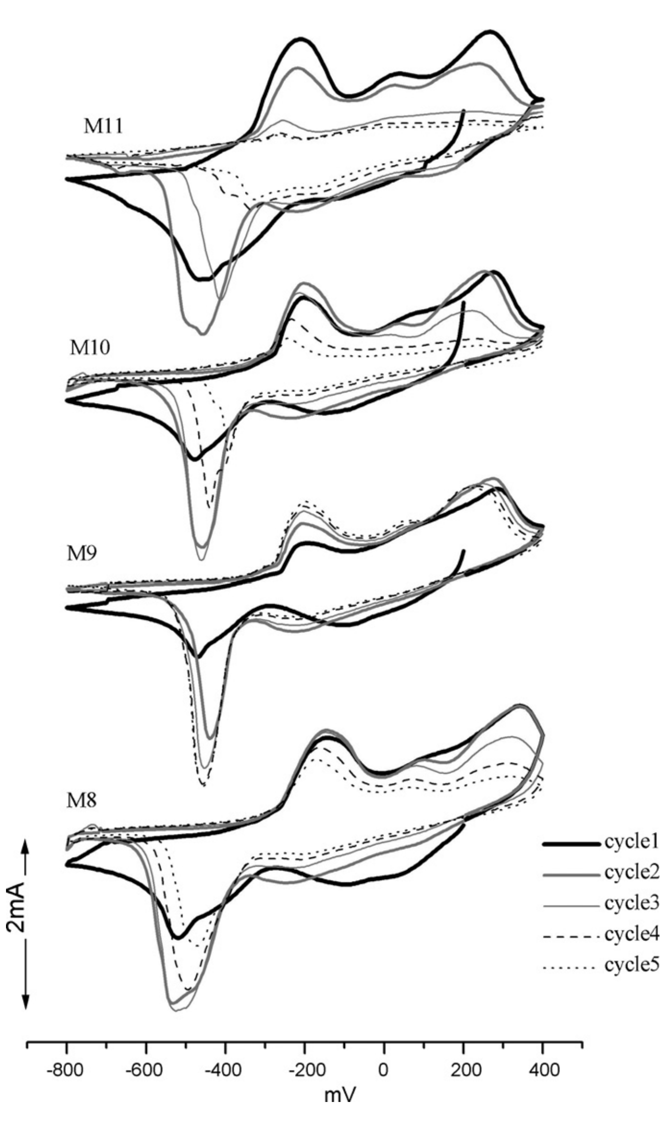

Fig. 13. Cyclic voltammograms of pcMDs carried out in a 9 M KOH. Scan rate was 0.25 mV s^{-1} vs. Hg/HgO reference electrode aqueous electrolyte. Samples are electrodeposited at a fixed frequency of 500 Hz and different duty cycles: $\theta = 0.1$ (M8); $\theta = 0.25$ (M9); $\theta = 0.5$ (M10) and $\theta = 0.75$ (M11).

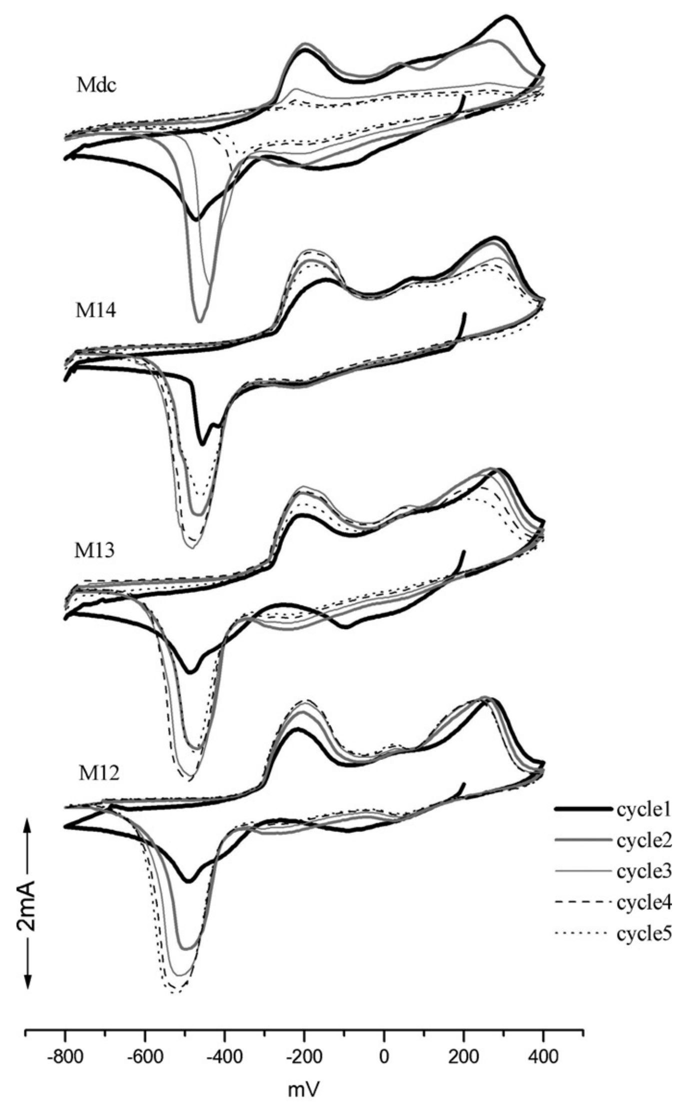

Fig. 14. Cyclic voltammograms of EMDs deposited by direct current (Mdc) and pulse current (pcMDs). pcMDs were electrodeposited at a constant pulse frequency of 1000 Hz and different duty cycles: $\theta = 0.25$ (M12), $\theta = 0.5$ (M13) and $\theta = 0.75$ (M14). Scan rate was 0.25 mV s^{-1} vs. Hg/HgO reference electrode.

dissolution of the starting material. The positive potential scan started from an initial voltage of 0.25 V followed by a shoulder beginning near 0 V leading consequently to the formation of δ-MnO_2.

The characteristics behavior of batteries with a lower cycle life could be clearly observed in CVs of the corresponding EMD samples (Figs. 13 and 14). Depending on the quality of EMD, loosing of Mn(III) species leads to a decrease in peak current intensities specially that of the first anodic peak and the second cathodic peak. The extent of such suppression of the latter peak is believed to be correlated to the magnitude of cycle life of batteries. In accordance to this statement, this suppression could be seen in all samples except for M9 and M12. M14 shows from the beginning a lower electrochemical activity as indicated in Fig. 14 by low energy drawn from the first reduction peak. The non-stability of EMD samples during cycling could also be observed through the suppression of the second anodic peak clearly observable in M8, M10, M11 and Mdc. In these samples, higher capacities of the first cathodic peak could be drawn in the first scan. This is correlated with the results of the corresponding batteries, which shows higher cycle capacities in the early 15–20 cycles. However, all reduction and oxidation peak currents are suppressed after the second scan. The extent of such suppression seems to be lower in M13. As could be seen in voltammogram, for samples produced at low duty cycles as in the case of sample M8 (θ: 0.1), the cathodic peaks are shifted to more negative values and both anodic peaks are shifted to more positive values. These phenomena are related to the presence of mix crystals as confirmed by XRD measurements (Fig. 1).

7. Conclusion

An efficient method for the synthesis of novel EMD was applied by using optimum conditions of pulse current electrodeposition. Results indicated that the cycle life of RAM batteries could be improved up to 230 cycles at lower bath temperatures of 80 °C than the conventional DC method carried out in boiling electrolyte solution. $M9_{LT}$ (bath temperature 60 °C) has actually shown a higher cycle life compared to Mdc_{HT} (bath temperature 98 °C). XRD patterns reveal that the formation of mix crystals occurs preferably for samples produced under application of duty cycles in the range of $\theta \geq 0.75$, the degree of crystallinity of EMD were decreased and the rate of defects formation increased.

Functional improvements may result from the combined effects of enhanced kinetics and current distribution leading to formation of more fine-grain-sized deposits and decreased formation of cracks. On the other hand, we suggest that under optimized PCD conditions, formation of fine distributed and poorly crystallized α- and/or β-MnO_2, may contribute to a higher structural stability through a wide range of pulse parameters.

Results indicate that current efficiencies significantly decrease upon decreasing t_{on}/t_{off} or decreasing duty cycles. The effect of the latter parameter on physico-chemical properties of deposits and electrochemical cycle performances is more influential than other pulse parameters. For example, we measured a rather poor cycle performance of all samples, which are produced at $\theta \leq 0.1$ (M2) and $\theta > 0.9$ (M1). For the latter, we found a high fraction of cation vacancies, which may be related to a facilitated proton transport due to the presence of higher fraction of incorporated water in deposits. In contrary, M2 contained low fractions of water molecules.

In order to further enhance the electrochemical performances and economical benefits of Manganese dioxide, more detailed PCD experiments should be conducted under low bath temperatures. In this regard, a precise optimization of this kind of investigation requires a modeling of the electrochemical phenomena and computation of the results.

References

[1] K.V. Kordesch (Ed.), Batteries, vol. 1, Marcel Dekker, 1975.
[2] P. Ruetschi, R. Giovanoli, P. Burki, in: Manganese Dioxide Symposium (compiled by A. Kozawa, R.J. Brodd), vol. 1, LC, Sample Office, Union Carbide Corpn., Cleveland Ohio, USA, 1975, p. 12.
[3] K.V. Kordesch, A. Kozawa, US Patent 3,945,847 (1976).
[4] J.B. Fernandes, B.D. Desai, V.N. Kamat Dalal, Electrochim. Acta 29 (1984) 181.
[5] M. Ghaemi, R.K. Ghavami, L. Khosravi-Fard, M.Z. Kassaee, J. Power Sources 125 (2004) 256.
[6] A. Susana Pilla, M.M.E. Duarte, C.E. Mayer, J. Electroanal. Chem. 569 (2004) 7.
[7] W. Kucza, Electrochem. Commun. 4 (2002) 669.
[8] N.S. Qu, D. Zhu, K.C. Chan, W.N. Lei, Surf. Coat. Technol. 168 (2003) 123.
[9] P.E. Bradley, D. Landolt, Electrochim. Acta 45 (1999) 1077.
[10] T. Nakanishi, M. Ozaki, H.-S. Nam-Seung Nam, T. Yokoshima, T. Osaka, J. Electrochem. Soc. 148 (2001) c627.
[11] M. Ghaemi, L. Khosravi-Fard, J. Neshati, J. Power Sources 141 (2005) 340.
[12] D.J. Kim, Y.M. Roh, M.H. Seo, J.S. Kim, Surf. Coat. Technol. 192 (2005) 88.
[13] K.R. Murali, V. Swaminathan, J. Appl. Electrochem. 32 (2002) 1151.
[14] S. Tao, D.Y. Li, Nanotechnology 17 (2006) 65.
[15] H. Kim, N.P. Subramanian, B.N. Popov, J. Power Sources 138 (2004) 14.
[16] A. Marlot, P. Kern, D. Landolt, Electrochim. Acta 48 (2002) 29.
[17] Y. Liu, Q. Fu, C. Pan, Carbon 43 (2005) 2264.
[18] M. Ghaemi, L. Binder, J. Power Sources 111 (2002) 248.
[19] K.H. Choi, H.S. Kim, T.H. Lee, J. Power Sources 75 (1998) 230.
[20] Y. Mastai, G. Hodes, J. Phys. Chem. B 101 (1997) 2685.
[21] D.D. Shivagan, P.M. Shirage, N.V. Desai, L.A. Ekal, S.H. Pawar, Mater. Res. Bull. 36 (2001) 607.
[22] N. Tantavichet, M.D. Pritzker, Electrochim. Acta 50 (2005) 1849.
[23] P. Ruetschi, J. Electrochem. Soc. 131 (1984) 2737.
[24] D.K. Walanda, G.A. Lawrance, S.W. Donne, J. Power Sources 139 (2005) 325.
[25] K.J. Vetter, N. Jaeger, Electrochim. Acta 11 (1966) 401.
[26] E. Preisler, K.V. Kordesch, A. Kozawa (Eds.), Proceedings of the Second Symposium on Battery Materials, vol. 2, IBA Inc., Cleveland, 1985, p. 247.
[27] Y. Matsumoto, M. Noguchi, T. Matsunaga, J. Phys. Chem. B 103 (1999) 7190.
[28] B. Pr'elot, F. Villi'eras, M. Pelletier, A. Razafitianamaharavo, F. Thomas, C. Poinsignon, J. Colloid Interface Sci. 264 (2003) 343.
[29] Y. Paik, J.P. Osegovic, F. Wang, W. Bowden, C.P. Grey, J. Am. Chem. Soc. 123 (2001) 9367.
[30] D. Landolt, A. Marlot, Surf. Coat. Technol. 169 (170) (2003) 8.
[31] Y. Chabre, J. Pannetier, Prog. Solid St. Chem. 23 (1995) 1.
[32] J.R. Hill, C.M. Freeman, M.H. Rossouw, J. Solid State Chem. 177 (2004) 165.
[33] E. Preisler, Electrochim. Acta 26 (1981) 1389.

[34] D. Qu, Electrochim. Acta 49 (2004) 657.
[35] S.K. Ghosh, A.K. Grover, G.K. Dey, M.K. Totlani, Surf. Coat. Technol. 126 (2000) 48.
[36] R.K. Sharma, A.C. Rastogi, K. Jain, G. Singh, Physica B 366 (2005) 80.
[37] J.C. Puippe, F. Leaman (Eds.), Theory and Practice of Pulse Plating, Am. Electroplaters Soc., Florida, 1986.
[38] R. Patrice, B. Ge'rand, J.B. Leriche, L. Seguin, E. Wang, R. Moses, K. Brandt, J.M. Tarascona, J. Electrochem. Soc. 148 (2001) A448.
[39] C.C. Wan, H.B. Linford, H.Y. Cheh, J. Appl. Electrochem. 9 (1979) 29.